# Impact of initial structural heterogeneity on long-term swelling behavior of MX80 bentonite pellet/powder mixtures

Agustín Molinero Guerra, Nadia Mokni, Yu-Jun Cui, Pierre Delage, Anh Minh A.M. Tang, Patrick Aimedieu, Frédéric Bernier, Michel Bornert

Canadian Science Publishing | Canadian Geotechnical Journal

# Impact of initial structural heterogeneity on long term swelling behavior of MX80 bentonite pellet/powder mixtures



| | |
|---|---|
| Journal: | *Canadian Geotechnical Journal* |
| Manuscript ID | cgj-2018-0301.R2 |
| Manuscript Type: | Article |
| Date Submitted by the Author: | 22-Mar-2019 |
| Complete List of Authors: | Molinero Guerra, Agustin; Institut de Radioprotection et de Surete Nucleaire<br>Mokni, Nadia; Institut de Radioprotection et de Surete Nucleaire,<br>Cui, Yu-Jun; Ecole des Ponts ParisTech<br>Delage, Pierre; Ecole des Ponts ParisTech<br>Tang, Anh Minh; Ecole des Ponts ParisTech,<br>Aimedieu, Patrick; ENPC,<br>Bornert, Michel; Ecole des Ponts ParisTech |
| Keyword: | heterogenous strcutural distribution, Microfocus X-ray Computed Tomography, Sealex in situ tests, MX80 bentonite pellet powder mixture |
| Is the invited manuscript for consideration in a Special Issue? : | Not applicable (regular submission) |
| | |

# Impact of initial structural heterogeneity on long term swelling behavior of MX80 bentonite pellet/powder mixtures

Agustín Molinero Guerra[1,2], Nadia Mokni[2*], Yu-Jun Cui[1], Pierre Delage[1], Anh Minh Tang[1], Patrick Aimedieu[1], Frédéric Bernier[3], Michel Bornert[1]

[1]Ecole des Ponts ParisTech, Laboratoire Navier/CERMES, Marne La Vallée, France
[2]Institut de Radioprotection et de Sûreté Nucléaire (IRSN), Fontenay-aux-Roses, France
[3]Agence Fédérale de Contrôle Nucléaire (AFCN), Belgium

*Corresponding author

Dr. Nadia Mokni

E-mail: nadia.mokni@irsn.fr

**Abstract:**

To better understand SEALEX in situ tests result´s carried out at Tournemire Underground Research Laboratory , the hydro-mechanical behavior of a pellet/powder MX80 bentonite mixtures prepared at a dry density of 1.49 Mg/m$^3$ were investigated by means of μ-CT observations and laboratory small scale infiltration tests. Radial and axial swelling pressures as well as relative humidity were monitored while wetting. Two configurations were considered: for the first, a pellet/powder mixture was prepared following a specific protocol to minimise initial structural heterogeneity; the second one was specially designed to study a strong heterogeneous mixture distribution. μ-CT observations performed on the two samples during hydration revealed an apparently homogeneous sample for the first mixture after 100 days of hydration. For the second specimen, several voids were still observed after 40 days of hydration. A comparison was made between the in situ and mock-up tests. It was observed that the evolutions of radial and axial swelling pressures depend on the initial heterogeneous distribution of the mixture. This heterogeneity is due to the different dry density values at the vicinity of the different sensors. The final values of axial swelling pressures were different for both configurations for the same global dry density.

**Keywords:** heterogenous structural distribution, Microfocus X-ray Computed Tomography, Sealex in situ tests, MX80 bentonite pellet powder mixture

## 1. Introduction

Bentonite high density pellet and powder mixture is being evaluated as possible sealing materials in deep geological repositories. In spite of the operational advantages related to the use of the mixture (e.g. ease of handling and minimisation of technological gaps), structural heterogeneities resulting from the installation process constitutes a matter of concern and require special approaches to adequately describe the material behaviour during hydration. In

this context, the Institute of Radiation protection and Nuclear Safety (IRSN) has launched SEALEX project to investigate the long-term hydraulic performance of sealing systems in normal and critical scenarios, as well as different core compositions. A series of *in-situ* experiments have been performed in IRSN's Underground Research Laboratory (URL – Tournemire, France) (Mokni & Barnichon, 2016; Mokni, 2016). This work focuses on the last sealex test in which a mixture of pellets and powder of bentonite with a proportion of 80/20 in dry mass was investigated. Based on the design of the in-situ experiments, two laboratory mock-up tests ($1/10^{th}$ scale) were performed aiming at studying the hydro-mechanical behavior and the structure changes of the material during hydration.

The hydro-mechanical behavior of different configurations of sealing plugs has been investigated at both laboratory and field scales (Mokni & Barnichon, 2016; Mokni, 2016, Wang et al., 2012, 2013; Saba et al., 2014). The relationship between swelling pressure and bentonite dry density of the material is an important result from these investigations (Börgesson et al., 1996; Dixon et al., 1996; Lloret et al., 2003; Imbert and Villar, 2006; Karnland et al., 2008; Gens et al., 2011; Villar et al., 2012 ; Wang et al., 2013; Saba et al., 2014; Schanz & Al-Badran, 2014). However, this relationship was mainly established based on the axial swelling pressure of the bentonite-based materials, and a few results of radial swelling pressure were considered for this purpose. Additionally, very few experiments focused on the evolution of dry density heterogeneity upon hydration and its influence on the swelling behavior. Furthermore, few investigations have been conducted on the hydro-mechanical behavior of bentonite pellet/powder mixture which is one of candidate sealing materials (Imbert and Villar, 2006; Van Geet et al. 2005; Molinero et al. 2016). This material, consisting of a mixture of low-density bentonite powder and highly compacted bentonite pellets, is obviously highly heterogeneous in its initial state. Molinero et al., (2016) demonstrated that preparing samples of a mixture of MX 80 bentonite pellet/powder at the

same target dry density with the same fabrication protocol does not ensure an initial homogenous structural distribution. The degree and distribution of heterogeneity might vary during hydration; thus, the average dry density might be not sufficient to characterize its final state. Another important characteristic of the bentonite mixture is the multimodal nature of its porous network which governs its overall hydromechanical properties.

The aim of this work is to investigate the effect of initial heterogeneous structural distributions on the swelling capacity and microstructural evolution of the bentonite pellet/powder mixture upon hydration. To account for possible structural heterogeneities resulting from the installation process in real disposal repositories, two configurations were considered. In the first configuration, the specimen consists of a mixture of MX80 bentonite pellet and powder with a proportion of 80/20 in dry mass, similarly to the SEALEX in-situ test. Special effort has been made to minimize initial structural heterogeneities. In the second configuration, a highly heterogeneous specimen, with half consisting of MX80 bentonite pellet and half of MX80 bentonite pellet/powder mixture was tested. The results of the small scale tests are presented along with the results of *in situ* SEALEX test. Comparison of the small scale laboratory tests and the in-situ experiments provides useful information regarding the test scale effect.



## 2. Materials

The studied soil is a mixture of MX80 bentonite pellet and powder (80/20 in dry mass). The bentonite investigated comes from Wyoming, USA. It was provided by the Laviosa-MPC company under the commercial name Expangel SP7 for pellets and SP30 for the powder. The MX80 bentonite has a smectite content of 80% with some inclusions of crystals (quartz, calcite and pyrite). The cation exchange capacity (CEC) is 98 meq/100g, with Na+ as major

exchangeable cation (52 meq/100g, with also 1.2 meq/100g for $K^+$, 10 meq/100g for $Mg^{2+}$ and 37 meq/100g for $Ca^{2+}$). The liquid limit is 560%, the plastic limit is 62% and the unit mass is 2.77 Mg/m$^3$ (Saba et al. 2014).

Pellets of bentonite were produced by Laviosa-MPC company by compacting a powder of MX80 bentonite in a mould of 7 mm in diameter and 7 mm in height. Compaction was performed at a water content of 6±1% by applying instantaneously the compaction effort, resulting in a pellet dry density $\rho_d$ = 2.06±0.06 Mg/m$^3$, corresponding to a void ratio $e$ = 0.30±0.07. The pellets were stored in the laboratory in a hermetic plastic box at 20°C. The initial suction ($s$ = 135 ± 3 MPa) was measured in the laboratory with a chilled mirror dew point tensiometer (Decagon WP4C), corresponding to an initial water content $w$ = 7.25%, slightly higher than the fabrication water content value (6±1%), due to further hydration after fabrication.

The MX80 bentonite powder was produced by crushing pellets. An initial water content of 3.17% was found in the laboratory after drying at 105°C for 24h, corresponding to an initial suction $s$ = 190.9 MPa (measured with a chilled mirror dew point tensiometer – Decagon WP4).

## 3. Methods

In order to investigate the HM behavior of the mixture an in situ test and four mock up infiltration tests have been performed. At small scale, two kind of experimental cells have been designed: two stainless steel cells equipped with relative humidity and swelling pressure sensors to investigate the macrostructural hydro-mechanical behaviour of the material and two Polymethyl methacrylate cells to investigate microstructural changes of the mixture while wetting by means of Microfocus X-ray Computed Tomography (µ-CT) observations. µ-CT is a non desctructive 3D imaging technique increasingly used to investigate various materials

intended as geological and engineered barriers in deep geological repositories like Boom and Opalinus clays (e.g. Chen et al 2014; Van Geet et al., 2008), compacted bentonite (e.g. Kozaki et al., 2001; Suuronene et al., 2014), and compacted bentonite mixtures (Van Geet et al, 2005; kawaragi et al., 2009; Saba et al., 2014).

## 3.1. SEALEX in situ test

The last SEALEX in-situ performance test namely PT-N4 has been performed, aiming at investigating the long term homogenisation of seals composed of the mixture of MX80 bentonite pellets and powder. When installing the experiment, a horizontal borehole (0 ± 2°), with a 60 cm diameter and 540 cm long was prepared by excavation in the Tournemire URL operated by IRSN, located in a Mesozoic sedimentary basin on the western edge of the French Causses ( Mokni et al., 2016). The bentonite-based core with a total length of 120 cm consists of a granular mixture of bentonite pellets and powder in a ratio of 80/20 (in dry mass). The bentonite core was constructed using an auger conveyor; vibration was applied through the auger itself in order to achieve the target dry density of 1.49 $Mg/m^3$.

The core was confined between two fixed stainless steel lids, namely upstream and downstream lids, which provided both hydraulic and mechanical closures (Figure 1). The lids consist of a stainless steel circular plate and a cylindrical stainless steel tube welded all around its periphery. It has a series of three rubber inflatable cushions (O-ring) all around and passing for the hydration tubings. The hydration at both sides of the lids (upstream and downstream) is based on special geotextile mats fed with water distribution tubes. The reduction in thickness of the mats due to the swelling of the buffer is limited to 4 MPa. The hydration system is equipped with a water distribution panel fed by a weighed stainless steel water tank connected with inflow lines to both hydration surfaces (downstream and upstream). The

confining system consists of a support tube inserted into the cylindrical tube of the downstream lid up to rest against the circular plate and of a closure plate (1400 mm in diameter) placed at the outer face of the borehole and secured by four bolts anchored to the rock.

In order to avoid potential flow paths along cables and sensors, and thereby, to limit the disturbance of the clay core as much as possible, wireless sensors were used. Three types of sensors were installed within the seal: 5 total pressure cells (Kulite BG-1-0234-6 MPa), 8 pore pressures sensors (Kulite ETM-200-375-1 MPa) and 8 relative humidity sensors (commercially-available Sensirion SHT75) (Figure 2). Three total pressure sensors were installed on the surface of the core at 60 cm from the downstream saturation face in order to measure the radial swelling pressure. Two total pressure sensors were installed at 0 and 120 cm from the downstream saturation face to measure axial swelling pressure. Hydration was performed by injecting synthetic water with the same chemical composition as the pore water of the Callovo-Oxfordian claystone from the ANDRA underground research laboratory in Bure (Table 1). Injection was carried out using a counter pressure of 0.2 MPa during few hours, and then the backward pressure was released.



### *3.2.* Experimental mock-up tests

*Mock-up tests to investigate microstructural evolution of the mixture*

The evolution of the microstructural distribution of the material upon hydration was investigated by means of Microfocus X-ray Computed Tomography observations (μ-CT). A special set-up consisting of a transparent PMMA (Polymethyl methacrylate) cell was designed (Figure 4). It has 60 mm of inner diameter and 120 mm of height, which corresponds to 1/10$^{th}$ scale of the SEALEX *in situ* tests. The mixture is prepared inside the cell, between two pore stones and filter papers. The rigid PMMA cell (30 mm thick) and the blocked piston ensure a

constant-volume hydration condition. The mixture is saturated from both top and bottom sides, as in the SEALEX *in situ* experiments. More details on the experimental cell could be found in Molinero et al., (2018).

μ-CT scans were carried out on both mixtures at initial state and during hydration by using an "Ultratom" microtomograph (RX Solutions, France). Images were reconstructed using the software Xact (RX Solutions). The source is a microfocus X-ray tube Hamamatsu L10801 and the imager is a Paxscan Varian 2520V (1960 x 1536 square pixels 127 μm size).

The X-ray source parameters were 160 kV and 120μA; the voxel size was 50 μm. The samples were scanned using 5760 projections in helical mode. After reconstruction, 2800 horizontal slices were obtained (16 bit images, 1499 x 1499 pixels). An external metal filter consisting of a 1.5mm thickness cooper plate was used in the μ-CT source. This filter allows reducing the low energy photon component of the X-ray beam, reducing the beam hardening effect.



*Mock-up tests to Investigate hydro-mechanical behavior of the mixture*

Two identical small-scale infiltration cells (mock-up tests, Figure 3) were designed in order to investigate the hydro-mechanical behavior of the mixture. The dimensions correspond to 1/10 of in situ SEALEX experiments (60 mm in diameter and 120 mm in height). The confined saturation conditions for the pellet/powder bentonite mixture are ensured by a rigid structure and a piston blocked by a screw. The material was saturated from both sides (top and bottom) as in the SEALEX *in situ* experiment. Six total pressure sensors were installed in the cell (SP20, SP40, SP60, SP80 and SP100), which allowed the measurement of the radial swelling pressures at different positions (h = 20, 40, 60, 80, and 100 mm from the bottom side). The accuracy of the sensors is ±1%. A force transducer was installed under the cell base, monitoring the axial swelling pressure. The relative humidity was also recorded by using five

199 relative humidity sensors (RH31, RH51, RH71, RH91 and RH111) placed at different heights
200 in the cell (h = 31, 51, 71, 91 and 111 mm, see Figure 3).

201

202 *Sample preparation and adopted protocol*

203

204 To account for possible structural heterogeneities resulting from the installation process in
205 real disposal conditions, two configurations were considered at the same global dry density of
206 1.49 Mg/m$^3$. In the first configuration, the specimen (samples 1 and 1a) consists of a mixture
207 of MX80 bentonite pellet and powder with a proportion of 80/20 in dry mass, similarly to
208 SEALEX in-situ test. A special preparation protocol was adopted to minimize initial structural
209 heterogeneities in terms of particle arrangement (Molinero Guerra et al., 2016). It consists in
210 filling the cell by packets corresponding to one layer of pellets spread over the base of the
211 cylinder and by adding the corresponding amount of powder (taking into account the
212 proportion 80% pellets – 20% powder in dry mass) (Figure 5a). In the second configuration, a
213 highly heterogeneous specimen (samples 2 and 2a) consisting of a mixture of MX80 bentonite
214 pellet and powder prepared at different proportions was tested (Figure 5b). In this case, the
215 half bottom part of the cell was filled with a 66.7% pellet/33.3% powder mixture (proportions
216 in dry mass) – corresponding to a dry density of 1.79 Mg/m$^3$, to ensure that all inter-pellet
217 voids are filled with powder. On the contrary, the top half of the cell was filled with only
218 pellets of bentonite at a dry density of 1.19 Mg/m$^3$. The latter case simulates possible defects
219 that might results from *in situ* installation process (e.g segregation, existence of zones with an
220 assembly of pellets with no powder filling the voids or zones with an accumulation of
221 powder)

222 All the tests started by opening the water inlet valves. At the beginning, air in the base or in
223 the piston was evacuated by opening the air outlet valve until no air bubble was observed in

the pipes. Water was then injected through both the top and the bottom of the sample. Values of radial and axial swelling pressure as well as relative humidity were recorded automatically by a data logger. The volume of injected water was also monitored during hydration.

## 4. Mock up tests experimental results

*Microstructural observations*

The microstructural evolution during hydration was investigated by μ-CT observations on two MX 80 bentonite pellet and powder samples (named sample 1a and sample 2a). Sample 1a was prepared to minimise initial heterogeneities and sample 2a was strongly heterogeneous.

Figure 6 shows the vertical μ-CT sections of sample 1a at different times. The initial state shows the presence of larger voids between the pellet and the porous stone at the top of the mixture, most probably due to segregation during the sample fabrication. Note also the presence of large inter-pellet voids which are not filled with powder, particularly in the peripheral part of the specimen. After 2 days of hydration, the top large inter-pellets voids are completely sealed due to the vicinity to the hydration front. During hydration, the poly-disperse assembly of the highly compacted pellets and powder is progressively lost. Inter-pellet voids are still observed after 56 days of hydration, even though the pellets located at the furthest position from both hydration fronts have already swollen at this time. An apparently global homogeneous sample is observed after 100 days of hydration at the considered resolution (50 μm/voxel). At this time, almost all the voids are completely sealed.

Figure 7 shows a zoom of an assembly of pellets located at the middle of sample 1a. These observations allow better understanding the pellets structural changes during hydration. After 11 days of hydration, liquid water has not reached this section but hydration is ensured by vapor transfer. Several cracks can be observed within the pellets. These cracks will play the role of preferential paths for vapor transfer during saturation. After 27 days, new cracks are

observed and the pellets are progressively degraded. The initial granular structure is almost lost after 56 days but some inter-pellet voids are still observed.

Figure 8 shows the vertical μ-CT sections of the highly heterogeneous sample 2a during wetting. A clear distinction can be observed between the top and bottom halves of the sample. For the 100-pellt/0-powder mixture (situated between 60 mm and 120 mm from the bottom hydration front), the initial granular structure completely disappears after 1 day of hydration. Pellets shape can be hardly distinguished; but several large voids can still be observed. After 40 days, the voids are almost sealed by swollen bentonite. A view of the structural evolution of the mixture at a horizontal section located within the looser upper part of the sample at 110 mm from the bottom hydration front is shown in Figure 9. Initially, an assembly of pellets with larger inter-pellet voids not filled with powder can be observed. After 30 min of hydration, the shape of pellets is completely lost as they swell instantaneously. After 90 min of hydration, all voids are completely sealed, resulting in an apparently homogeneous bentonite mixture. More details on image analysis of μ-CT observation of sample 1a could be found in Molinero et al. (2018)

For the denser lower part of sample 2a ( 66.7-pellet/33.3-powder), only pellets in contact with the bottom porous stone start swelling after 1 day of hydration, but no significant changes are observed in the rest of the sample (Figure 14). Unlike the looser upper part of the sample where the material was rapidly inundated with water, for the denser lower part it is suspected that saturation occurs by advection of liquid water and diffusion of vapor. After 5 days, a homogenous saturated bentonite layers is formed at the bottom boundary of the sample. At this layer, large macro voids are invaded by the swollen bentonite and the hydraulic conductivity becomes very low, favoring the saturation of the remaining unsaturated zones by vapor transfer. Interestingly, the material located at the limit between the denser and looser part (at 60 mm from the bottom) starts swelling rapidly after 5 days since it

is also hydrated by water coming from the looser part. Significant changes are observed after 35 days. In the looser part, most inter-pellets voids are already sealed, while in the denser part an increase of the thickness of the outer apparently homogenous bentonite layer is observed. However, after 40 days, several inter-pellets voids are still identified in the looser part; but they are progressively sealed, as it is observed within the outer layer closer to the hydration front (Figure 15). Simultaneously, at the denser part of the sample, the pellet shape can be still noticeable. Unfortunately, the µ-CT observations were stopped at 40 days.

*Mechanical results*

Figure 10 displays the swelling pressure evolution of the two investigated samples (sample 1 and 2) after 300 days of hydration. Two distinct hydro-mechanical responses can be identified for both mixtures. For sample 1 (Figure 10a), the pattern of behavior is very similar in all positions ( SP 20, 40, 60, and 80). The swelling pressure increases at different rates depending on the distance to the hydration front, then reaches a nearly stationary value after 200 days. Nevertheless, a negative rate is observed at the beginning of the hydration process at SP40. This negative rate can be related to a rearrangement of the material structural distribution at this zone at the beginning of the hydration process. After 300 days, the highest radial swelling pressure (4.6 MPa) is measured at SP80 located at 40 cm from the top hydration face. At SP60 the magnitude of the swelling pressure is lower and reaches 3.8 MPa after 300 days. At SP100 located at 20 mm from the top hydration front a different behaviour is observed. The swelling pressure increases very rapidly and reaches a peak of about 2.1 MPa (a zoom is presented in Figure 11). After about 5 hours a significant decrease of the swelling pressure occurs, to a minimum value of 1.5 MPa. The swelling pressure increases again at slower rate and reaches a value of 2.55 MPa after 60 days. Afterwards, the swelling pressure increases and is stabilized at 3.3 MPa after 200 days. The peak occurrence followed by a decrease corresponds to the reorganisation of the microstructure characterized by the collapse of the

298 macrospores between the bentonite grains. It is worth noting that the horizontal swelling
299 pressure measurements are strongly influenced by the local microstructural distribution at the
300 vicinity of the sensors. The non-peak occurrence at SP40, SP60, and SP80 suggest that the
301 sensors were placed in zones where high density pellets are tightly arranged with few or no
302 grains of bentonite powder in between of them. Similar trends were observed for the axial
303 swelling pressure. However, in this case no macrostructural collapse is observed, indicating
304 that collapse in some zones is compensated by the non-collapsing behavior of other zones.

305 A different pattern of behavior is observed for the highly heterogeneous mixture (sample 2,
306 Figure 10b). At SP20 located within the denser bottom part of the mixture, a fast increase of
307 the swelling pressure is observed at the beginning of the test, reaching a peak value of 6.1
308 MPa. Then, it decreases until a value of 3.6 MPa after 75 days of hydration. Swelling pressure
309 increases slightly between 150 and 300 days of hydration, being 3.8 MPa the highest value.
310 On the contrary, at SP40 the swelling pressure increases gradually, and then reaches a nearly
311 stationary value after 100 days.

312 At SP60 located at the limit between the denser and the looser part of sample 2, a fast increase
313 of swelling pressure is recorded, with a rate higher than that at SP40, until reaching a peak at
314 1.6 MPa. Then, the swelling pressure decreases slowly to a value of 1.2 MPa. After 72 days,
315 an increase is observed again with the same rate as at SP40. After 300 days of hydration, a
316 swelling pressure of 2 MPa is measured.

317 The lowest swelling pressure increase rate and magnitude are observed at SP80 and SP100
318 respectively, located at the upper looser part of sample 2 (1.19 $Mg/m^3$), at 40 and 20 cm form
319 the upper hydration front. At SP80, the radial swelling pressure increases very slowly until
320 reaching a value of 0.3 MPa after 75 days of hydration. Then, an increase of swelling pressure
321 is observed until 100 days, where an almost constant value of 1.2 MPa is reached. The lowest
322 swelling pressure magnitude is recorded at SP100 where a value of about 0.6 MPa is reached

after 60 days and remains constant till 300 days. For all sensors, after 230 days a fluctuation is observed for all sensors, which could be due to problems in the system acquisition during the test.

For the axial swelling pressure, as in sample 1, it increases slowly and reaches a nearly stationary value after almost 100 days. However, in this case the magnitude of the swelling pressure in lower (1.1 MPa in this case against 2.3 MPa for sample 1).

Figure 12displays the profiles of swelling pressure at different times for both samples. For sample 1 (Figure 12a), the curves have a quasi-parabolic shape with a symmetry at 60 mm. This trend is not observed for the highly heterogeneous sample 2 (Figure 12b). In this case, the highest swelling pressure value is reached at the bottom of the mixture, in the denser part of the specimen. Figure 13 displays the swelling pressure profiles after 300 days of hydration for both samples. A relatively constant radial swelling pressure is observed for sample 1, in the range from 3.3 to 4.4 MPa. On the contrary for the highly heterogeneous sample 2, the swelling pressure tends to decrease from the bottom to top. The highest value is observed at 20 mm from the bottom hydration face, where the sample has a high initial density of 1.79 $Mg/m^3$.

*Hydraulic results*

Figure 14 shows the evolution of Relative Humidity (RH) measured at different distances from the hydration faces for both samples. For sample 1 (Figure 14a), once hydration started, the relative humidity at RH31 located at 31 mm from the bottom hydration face and at RH111 located at 9 mm from the top hydration face increases rapidly and reaches 100% after 20 and 13 days respectively. At RH71, located at 49 cm from the top hydration face started to increase, relative humidity started to increase after about 45 days, indicating that the increasing rate of RH is dependent on the distance from the wetting ends.

For sample 2 (Figure 14b), two patterns of behavior can be distinguished. For sensors RH71, RH91 and RH111 located within the upper looser part of the sample, RH increases instantaneously at the beginning of the test, reaching 100% for RH91 and RH111 and 80% for RH71. Then, a decrease is observed for the three sensors until 92%, 87% and 58% for RH111, RH91 and RH71, respectively. Subsequently, RH increases again until saturation at 4, 30 and 40 days for RH111, RH91 and RH71 respectively. Different trends are observed at RH51 and RH 31 located within the denser bottom part of sample 2. At these sensors RH increases progressively until reaching 100% after 20 (RH 31) and 40 days (RH 51), respectively.

The volume of injected water is displayed in Figure 15 for both samples. The top and bottom volumes of injected water were measured separately during the saturation process. In both cases, a higher volume is injected though the top due to the presence of larger voids at this level combined with the gravity effect. Additionally, larger water volumes were injected through the top and bottom for sample 2.

After 300 days, the total volume of injected water is 184.6 $cm^3$ for sample 1 and 230.4 $cm^3$ for sample 2. These volumes are higher than the theoretical water volume (155 $cm^3$) calculated by considering a global dry density of 1.49 $Mg/m^3$.

## 5. Comparative analysis and discussions

Since no information is available about the structural distribution of the bentonite pellet/powder mixture in SEALEX *in situ* test PTN4, comparison of the latter to both mock up tests, allows better interpretation of PTN4 results. The mock up tests are considered as extreme cases since they were performed on a highly heterogeneous sample (sample 2) and on an ideally prepared sample (sample 1) (specific preparation protocol to minimize the heterogeneities as much as possible).

*Injected volume of water*

371 The flooding phase in PTN4 was performed in 2 steps: First, a back pressure of 0.2 MPa was
372 applied, in 2 hours. Second, the back pressure was removed, and the upper level of the water
373 in the tank was constantly maintained at 1m above the axis of the borehole (*i.e.* 1 m water
374 head). Figure 16 shows the evolution of injected water volume over time. Interestingly, a
375 backward flow into the tank induced by bentonite swelling is observed. After a slight increase
376 in rate during the first months, the water intake slowed down to a very low rate and reached
377 95 L after 780 days. A close examination of the hydration system revealed the presence of
378 entrapped air within the hydration lines which prevented further water intake. Purging of the
379 tubings allowed for further water intake. A total amount of 125 L of synthetic water was
380 injected into the system after 1400 days.

381 In order to compare the evolution curves at different scales (PTN4 versus mock up tests), the
382 water volumes were normalized considering the maximum water volume that can be injected
383 in both mock up and *in situ* tests (158 l for PTN4, 0.158 l for mock up tests). Assuming that
384 the *in situ* test is an intermediate case in between the two extreme cases studied in the
385 laboratory (mock up 1 and 2), an up scaling time scale ratio of 30 (in situ/mock up tests) was
386 found from the normalized water volume (Figure 17).

387 Even though both mock up test samples were prepared at the same mean dry density, larger
388 injection rate and water volume were observed in sample 2. At the beginning of the test, the
389 injection rate is higher for sample 2 because the permeability is higher in the looser upper part
390 of the sample. The difference between injected water volume in sample 2 and the theoretical
391 value may be related to the low water density (1.00 $Mg/m^3$) considered. This value can be
392 much higher for high plasticity materials as the MX80 (Marcial, 2003; Villar and Lloret,
393 2004; Lloret and Villar, 2007; Jacinto et al., 2012).

394

*Relative humidity evolution*

In PTN4, 8 relative humidity sensors were installed in the bentonite core at 22, 52, 82 and 112 cm from the downstream hydration face (Figure 2). Sensors RH52 (1, 2) placed at 52 cm from the downstream lid was malfunctioning since the beginning of the hydration phase. Additionally, data from several operating sensors were not available during several time periods due to a temporary problem in the data acquisition units. The variations with time of relative humidity measured at different sections are displayed in Figure 18. In situ data are compared to those from both mock up tests using time scale factor of 30. Once the hydration started, at sensors RH22 (1,2) and RH112 (1,2) located at 22 and 112 cm from downstream hydration face in PTN4, the relative humidity increased progressively and reached 95% after 450 days. A faster RH increasing rate is observed in both mock up tests at sensor RH22 located closer to the bottom and top hydration faces, respectively. This difference is mainly attributed to the different sensors positioning within the in situ and laboratory tests. Indeed, in the mock up tests RH sensors were located at the interface between the sample and the cell, where there is almost no bentonite powder filling the inter-pellets voids (Figures 6 and 8), while in the *in situ* test RH sensors were installed in the bentonite-based core at a distance of about 12.5 cm from the host rock.

The µ-CT observations of sample 1 (Figure 6) revealed that after 56 days in the central zone of the sample pellets were clearly distinguishable, indicating that pellets swelling and hydration are still progressing. Nevertheless, RH measurements suggests full saturation of the mixture after almost 45 days ( Figure 14a). This indicates that the saturation of the highly compacted pellets (2.2 Mg/ $m^3$) is a slower process. This phenomenon was identified as water transfer between the macrostructure and the microstructure, the rate being controlled by several microstructural parameters (e.g. Gens et al, 2011, Alonso et al, 2011).

Different evolution trends are observed at RH82 (1,2) (Figure 18c). Similarly to RH71 and RH 91 located within the looser upper part in sample 2, a fast increase of RH is observed at the beginning of hydration until reaching 100%, prior to a rapid drop. Then, RH increases again gradually. This suggests that the structural distribution of the bentonite-based core at the vicinity of the RH sensors is comparable to the upper looser part in sample 2. Since no powder exists in this zone, this behavior can be associated to structural changes of the granular pellets during wetting: initially, water comes instantaneously through the large inter-pellet voids, which leads to rapid RH increase. Simultaneously, there is a water transfer from the large inter-pellet voids to the highly compacted pellets voids. As pellets saturation progresses, they lose their initial granular structure due to swelling, and invade the inter-pellet voids (Figures 8 and 9). The prevailing suction at the vicinity of the sensors is no longer the initial one measured just upon hydration but corresponds to that of the swollen pellets which is much higher. Saturation of the pellets is a slower process and RH increases again gradually.

*Swelling pressure evolution*

The in situ radial and axial swelling pressure evolutions are depicted in Figure 19and 20 respectively, together with the normalized curves of mock up tests. Figure 19 compares the evolution of PTN4 radial swelling pressure measured by three total pressure sensors installed on the surface of the bentonite core at 60 cm from the downstream saturation face. It is observed that the swelling pressures increased over time at different rates, depending on the sensors positions. The highest swelling pressure increasing rate is measured at sensor SP60 (1) located on the top of the radial cross section. The value reached at 1200 days is almost 2.4 MPa. On the contrary, the same lower swelling pressure evolutions rates are recorded at SP60 (2) and SP60 (3) and lower values are reached after 1200 days of hydration (1.3 MPa at SP60 (2) and 1.2 MPa SP60 (3)). The measured differences suggest a heterogeneous structural distribution within the *in situ* mixture core, resulting from the field installation process

adopted. This observation is confirmed when comparing the radial swelling pressures measured at the same position in both mock up tests: different swelling pressure increasing rates and magnitudes were measured even though both tested samples were fabricated at the same global dry density (1.49 $Mg/m^3$).

Figure 20 shows the evolution of axial swelling pressure measured by a sensor placed at the downstream hydration face in PTN4. No reliable data have been provided by the total pressure sensor at 120 cm, at the upstream hydration face. The plot shows that the swelling pressure increased at a constant rate and reached 1.4 MPa after 1200 days. Lower values are obtained in the laboratory mock up tests. This difference is closely related to the measurement methods. In the *in situ* test, the sensors placed at upstream and downstream measured the axial swelling pressures locally, while in the mock up tests, the force transducer installed under the cell base ensure the measurement of the global axial swelling pressure.



No peaks of swelling pressure are observed in the *in situ* test, while this particular behavior characterized by a peak occurrence followed by a decrease of the swelling pressure are observed in the mock up tests: at sensors SP100 (mock up 1) and SP20 (mock up 2), suggesting the appearance of local collapse of the macrospores between the bentonite grains in the latter case (Alonso et al., 2011; Gens et al., 2011). The non-peak occurrence in PTN4 suggests that the sensors were placed in zones where high density pellets are tightly arranged with a few or no grains of bentonite powder in between.

For both *in situ* and laboratory tests, the final values of axial swelling pressure are lower than those measured radially. A high anisotropic coefficient $C_a$ (defined as the horizontal swelling pressure divided by the axial pressure) ranging from 1.25 and 1.65 is obtained for mock up 1 (Figure 21). This means that sample 1 is only homogeneous in terms of particle arrangement but anisotropy of the soil fabric is not encountered. For mock up 2 (sample 2), the values of $C_a$ range from 0.5 to 2.9. This strong anisotropy is obviously induced by the highly

heterogeneous structural distribution in sample 2. Similarly in PTN4, significant Ca values are obtained (Figure 21), confirming that the installation process greatly influenced the structural distribution of the mixture. Different values are obtained for the three sensors located at 60 mm as their responses are different. The values are near one for SP60(1) and SP60(2) and between the two mock-up tests for SP60(3). This suggests that high heterogeneity exists in several zones PTN4, where pellets are assembled with no or few bentonite powder filling the inter-pellets large voids.

## 6. Conclusion

In the SEALEX project initiated by IRSN, the performance test PT-N4 was conducted to investigate the long term hydro-mechanical behavior of a mixture of pellet and powder of MX80 bentonite (80/20 in dry mass). In this test, the bentonite-based core was fully equipped with wireless sensors in order to measure the radial and axial swelling pressure as well as relative humidity at different positions during the saturation process. In parallel, 1/10 mock-up tests were performed in the laboratory in order to further investigate the effect of the initial structural distribution of the mixture on the HM behavior.

Two different samples were tested, aiming at investigating different possible responses depending on the initial pellet/powder distribution. The first one consists of a pellet/powder mixture with a proportion of 80/20 in dry mass, fabricated with a special protocol which allows a relatively homogeneous sample. The second one was specially fabricated to investigate a strong heterogeneous distribution: the lower half of the sample was prepared with a mixture in which all the inter-pellet voids were filled with grains of powder, while the upper half of the sample was filled only with pellets of bentonite. A heterogeneous evolution of the swelling pressure was found for both mixtures, especially for the second one, for which different swelling pressure values were found after 300 days of hydration. This heterogeneity

494 is due to the different initial dry density values in the vicinity of different sensors, which
495 depends on the pellet/powder distribution. The final value of axial swelling pressure was
496 different for both mixtures even though the global dry density was the same. This means that
497 the axial swelling pressure depends also on the pellet/powder distribution. Therefore, special
498 attention has to be paid to establish the relationship between swelling pressure and dry density
499 of the material, in which the axial swelling pressure is usually considered.

500 μ-CT observations carried out on the two samples while wetting revealed that an apparently
501 homogeneous sample was obtained for the first mixture after 100 days of hydration. However,
502 for the second specimen, several voids were still observed after 40 days of hydration,
503 concentrated in the looser part of the sample. No voids were observed in the horizontal
504 sections of the mixture near the hydration front for the looser part after 90 min of hydration.
505 Therefore, more time is necessary to reach a homogeneous sample for the second mixture.

506 A comparison was performed between the laboratory tests and the SEALEX in-situ test. A
507 factor scale of 30 was considered while comparing both tests, based on the volume of water
508 injected during wetting. The different protocols followed in order to obtain the in-situ mixture
509 and the investigated material in the laboratory explains the differences between the results,
510 especially for the axial swelling pressure.

511

512 # References

513 Alonso, E.E., Romero, E. and Hoffmann, C., (2011). Hydromechanical behavior of
514 compacted granular expansive mixtures: experimental and constitutive study.
515 Géotechnique 61 (4), 329–344.

516 Barnichon, J.D., Dick, P., Bauer, C., (2012). In: Qian, Zhou (Eds.), The SEALEX In-situ
517 Experiments: Performance Test of Repository Seals. Harmonising Rock Engineering and
518 the Environment. Taylor & Francis Group, London, pp. 1391–1394 (ISBN 978-0- 415-
519 80444-8).

Börgesson, L., Karnland, O. and Johannesson, L. E., (1996). Modelling of the physical behavior of clay barriers close to water saturation. Engineering Geology 41, 127–144.

Chen G.J, Maes, T., Vandervoort F., Sillen, X., Van Marcke P., and Honty, M., Dierick M. , Vanderniepen P.,(2014). Thermal Impact on Damaged Boom Clay and Opalinus Clay: Permeameter and Isostatic Tests with lCT Scanning. Rock Mech Rock Eng 47, 87–99.

Dixon, D. A., Gray, M. N. and Graham, J., (1996). Swelling and hydraulic properties of bentonites from Japan, Canada and the USA. Environmental Geotechnics 1, 43–48.

Gens, A., Vallejan, B., Sánchez, M., Imbert, C., Villar, M.V. and Van Geet, M., (2011). Hydro-mechanical Behavior of a Heterogenous Compacted Soil: Experimental Observations and Modelling.

Imbert, C. and Villar, M.V., (2006). Hydro-mechanical response of a bentonite pellets/powder mixture upon infiltration. Applied Clay Science, 32(3-4), pp.197–209.

Jacinto, A.C., Villar, M.V., Ledesma, A., (2012). Influence of water density on the water-retention curve of expansive clays. Geotechnique 62 (8), 657–667.

Karnland, O., Nilsson, U., Weber, H. and Wersin, P., (2008). Sealing ability of Wyoming bentonite pellets foreseen as buffer material – laboratory results. Physics and Chemistry of the Earth, Parts A/B/C 33, S472–S475.

Kozaki, T., Suzuki., S., Kozai., N., Sato., S., Ohashi, H., (2001) Observation of Microstructures of Compacted Bentonite by Microfocus X-Ray Computerized Tomography (Micro-CT), Journal of Nuclear Science and Technology, 38:8, 697-699.

Kawaragi, C., Yoneda, T., Sato, T., Kaneko, K., (2009) Microstructure of saturated bentonite characterized by X-ray CT observations. Engineering Geology, 106,51-57

Lloret, A., Villar, M. V., Sánchez, M., Gens, A., Pintado, X. and Alonso, E. E., (2003). Mechanical behavior of heavily compacted bentonite under high suction changes. Géotechnique 53, No. 1, 27–40.

Lloret, A., Villar, M., (2007). Advances on the knowledge of the thermo-hydro- mechanical behavior of heavily compacted FEBEX bentonite. Physics and Chemis- try of the Earth 32, 701–715.

Marcial, D., (2003). Comportement hydromécanique et microstructural des matériaux de barrière ouvragée. (PHD thesis) École Nationale des Ponts et Chaussées, Paris, France.

Mokni, N. & Barnichon, J.D., (2016). Hydro-mechanical analysis of SEALEX *in situ* tests-Impact of technological gaps on long term performance of repository seals. Engineering Geology, 205, pp. 81-92.

Mokni, N., (2016). Analysis of hydro-mechanical behavior of compacted bentonite/sand mixture using a double structure formulation. Environ Earth Sci (2016) 75: 1087. https://doi.org/10.1007/s12665-016-5872-2.

Molinero-Guerra, A., Mokni, N., Delage, P., Cui, Y. J., Tang, A. M., Aimedieu, P., Bernier, F., & Bornert, M., (2016). In-depth characterisation of a mixture composed of powder/pellets MX80 bentonite. *Applied Clay Science*.

Molinero-Guerra, A., Aimedieu, P., Bornert, M., Cui, Y. J., Tang, A. M., Sun, Z., Mokni, N., Delage, P., Bernier, F., (2018). Analysis of the structural changes of a pellet/powder bentonite mixture upon wetting by X-ray computed microtomography. *Applied Clay Science*, Volume 165, 2018, Pages 164 169, ISSN 0169-1317.

Saba, S., Cui, Y.J. and Barnichon, J.D., (2014). Investigation of the swelling behavior of compacted bentonite–sand mixture by mock-up tests. Canadian Geotechnical Journal, 51(12), pp.1399–1412.

Saba, S.,Delage, P., Lenoir, N., Cui, Y.J, Tang, A.M., Barnichon.(2014). Further insight into the microstructure of compacted bentonite–sand mixture. Engineering Geology Volume 168: 141-148.

Schanz, T. and Al-Badran, Y., (2014). Swelling pressure characteristics of compacted Chinese Gaomiaozi bentonite GMZ01. Soils and Foundations 54, No. 4, 748–759.

Suuronen, J.P., Matusewicz, M.,Olinb, M., Ritva Serimaa R., (2014). X-ray studies on the nano- and microscale anisotropy in compacted clays: Comparison of bentonite and purified calcium montmorillonite. Appl.Clay Sci. http://dx.doi.org/10.1016/j.clay.2014.08.015

Van Geet, M., Volckaert, G. and Roels, S., (2005). The use of microfocus X-ray computed tomography in characterising the hydration of a clay pellet/powder mixture. Applied Clay Science, 29(2), pp.73–87.

Van Geet, M., Volckaert, G. and Roels, S., (2005). The use of microfocus X-ray computed tomography in characterising the hydration of a clay pellet/powder mixture. Applied Clay Science, 29(2), pp.73–87.

Van Geet, M., Bastiaens, W., Ortiz L. (2008). Self-sealing capacity of argillaceous rocks: Review of laboratory results obtained from the SELFRAC project. Physics and Chemistry of the Earth 33:S396–S406.

Villar, M.V., Lloret, A., (2004). Influence of temperature on the hydro-mechanical behaviour of a compacted bentonite. Applied Clay Science 26 (1–4), 337–350.

Villar, M. V., Gómez-Espina, R. and Guitiérrez-Nebot, L., (2012). Basal spacings of smectite in compacted bentonite. Applied Clay Science 65–66, 95–105.

Wang, Q., Tang, A.M., Cui, Y.J., Barnichon, J.D. and Ye, W.M., (2013). A comparative study on the hydro-mechanical behavior of compacted bentonite/sand plug based on laboratory and field infiltration tests. Eng. Geol. 162, 79–87.

Wang, Q., Tang, A.M., Cui, Y.J., Delage, P. and Gatmiri, B., (2012). Experimental study on the swelling behavior of bentonite/claystone mixture. Eng. Geol. 124, 59–66. http://dx.doi.org/10.1016/j.engeo.2011.10.003.

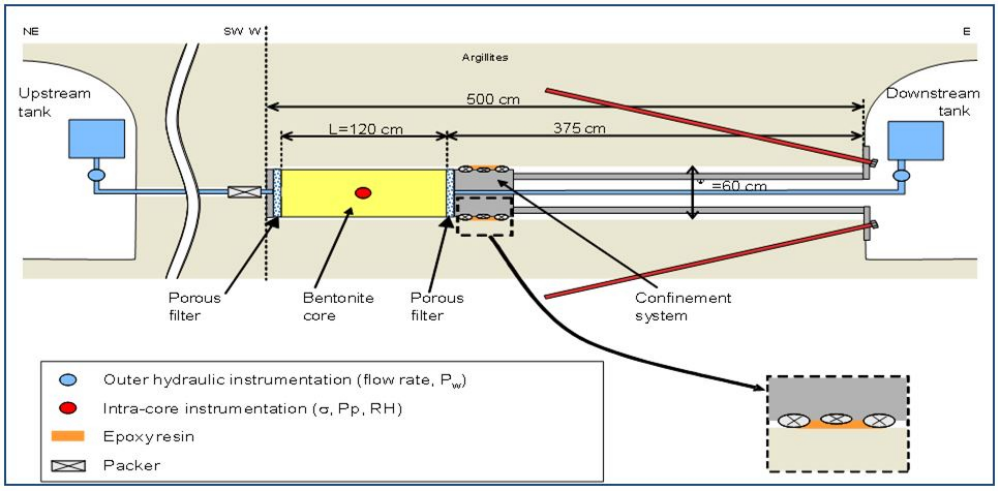


Fig. 1. Layout of the SEALEX in situ test (Modified from Mokni et al. 2016)

341x168mm (72 x 72 DPI)

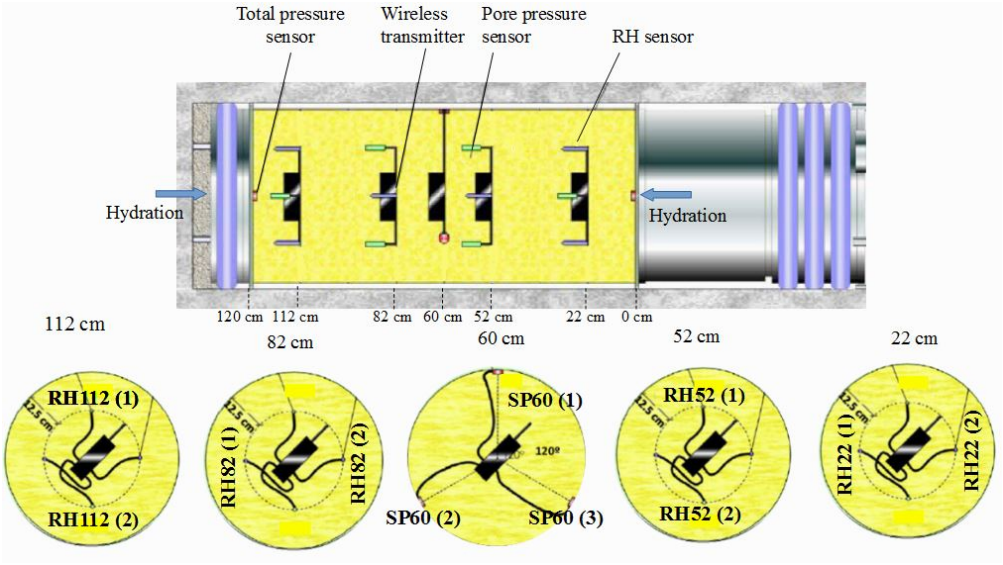


Fig. 2. Distribution of the relative humidity and swelling pressure sensors in the seal of SEALEX test.

355x200mm (72 x 72 DPI)

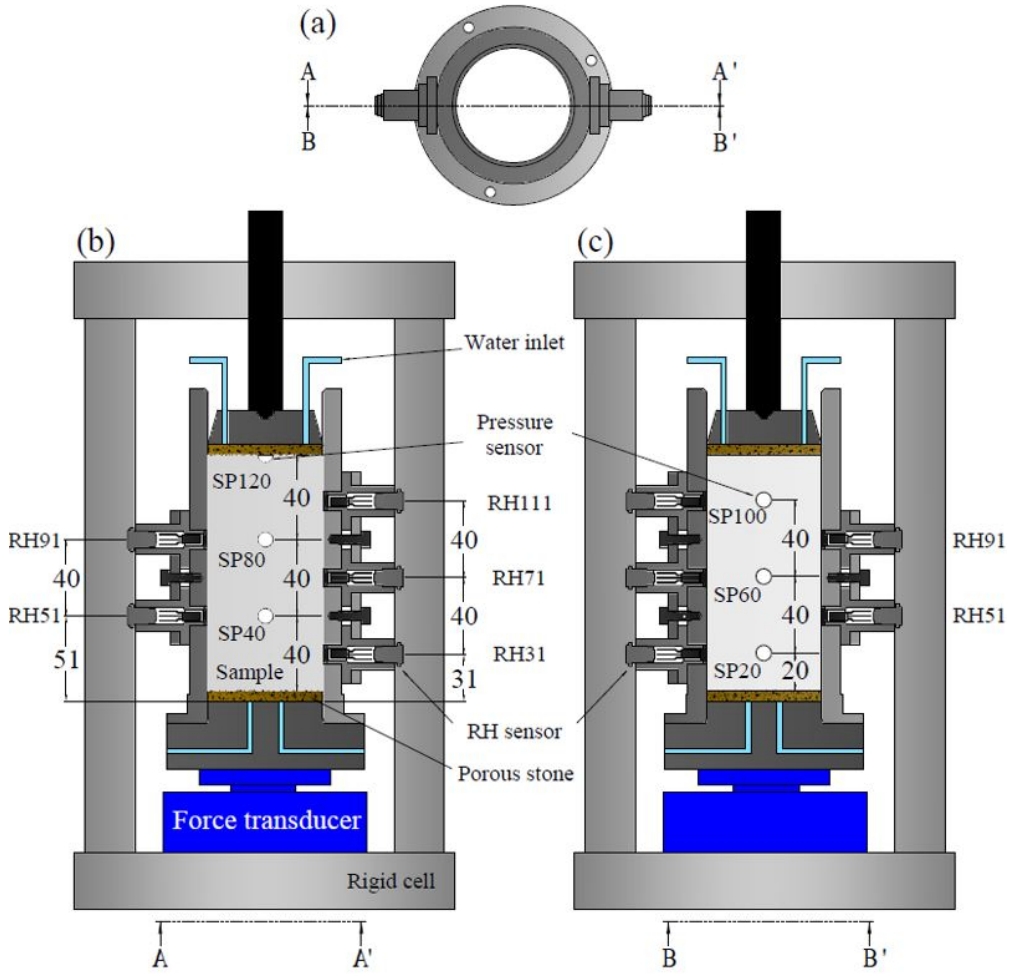


Fig. 3. Layout of the mock-up test cell (a) top view; (b) section A-A'; (c) section B-B'.

283x280mm (72 x 72 DPI)

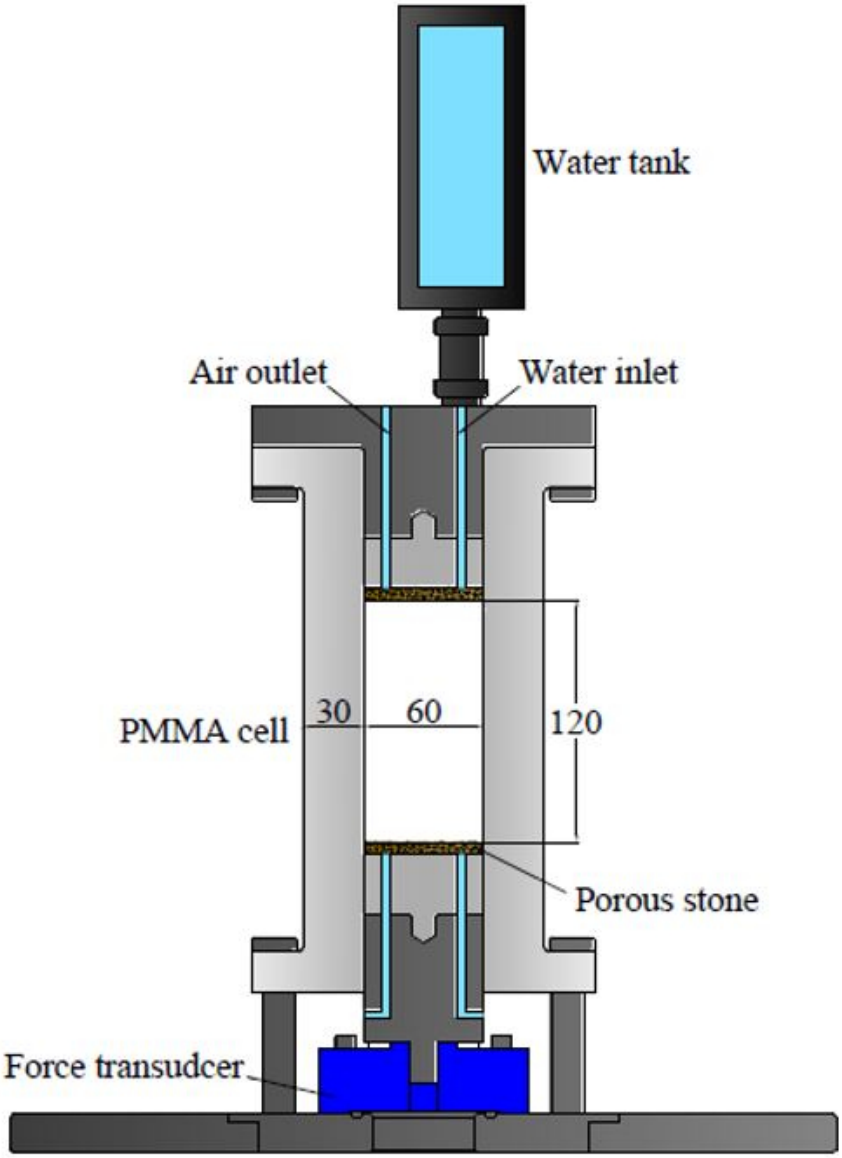


Fig. 4. Layout of the transparent PMMA cell.

175x242mm (72 x 72 DPI)

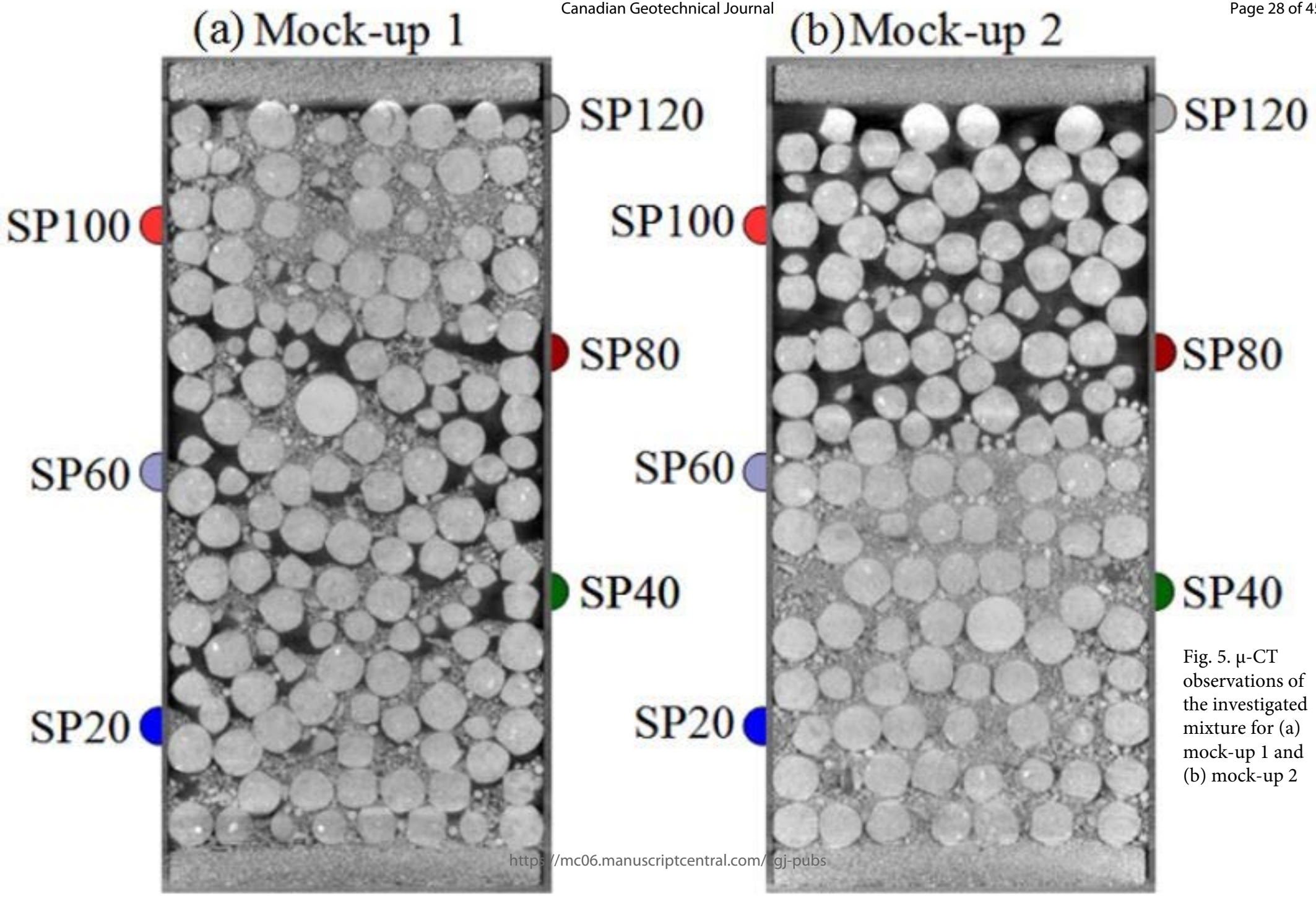


Fig. 5. μ-CT observations of the investigated mixture for (a) mock-up 1 and (b) mock-up 2

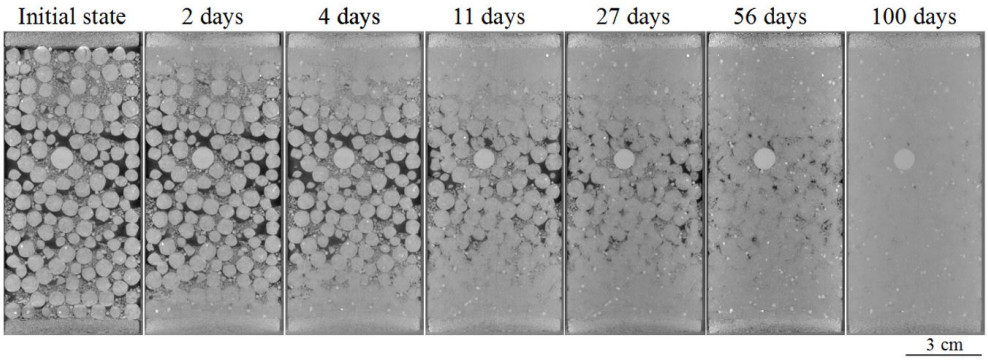


Fig. 6. Evolution of the patterns of vertical sections of sample 1a while wetting.

482x177mm (72 x 72 DPI)

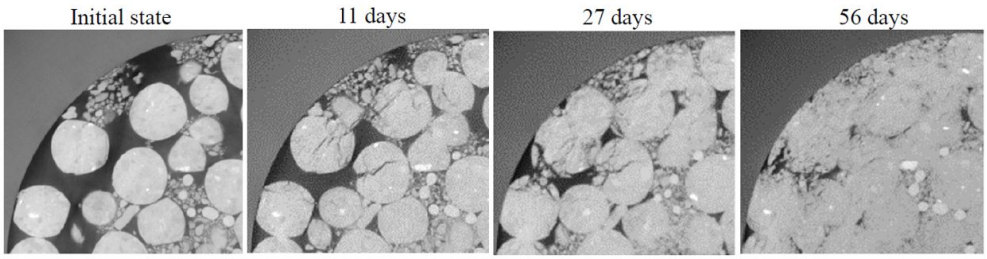


Fig. 7. Zooms at 60 mm from the bottom of the sample1a at different times.

443x117mm (72 x 72 DPI)

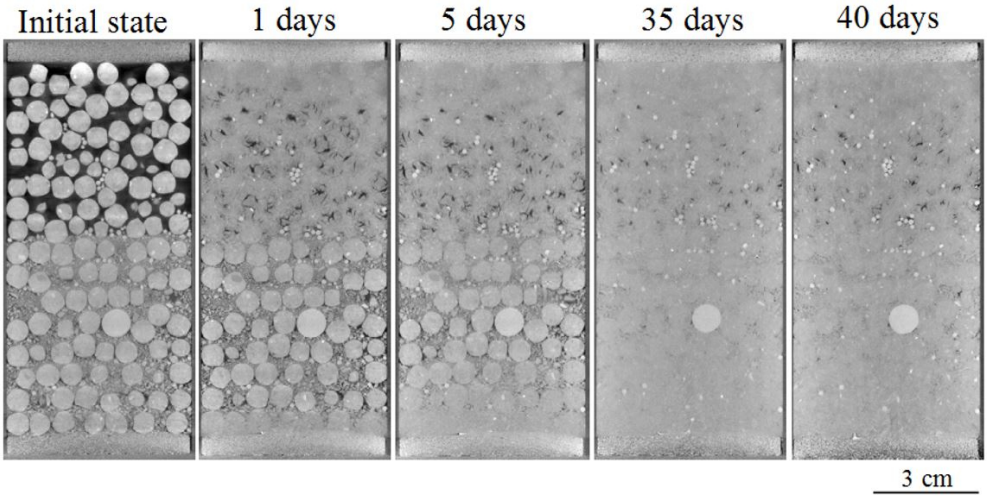


Fig. 8. Evolution of the patterns of vertical sections of sample 2a upon wetting.

408x210mm (72 x 72 DPI)

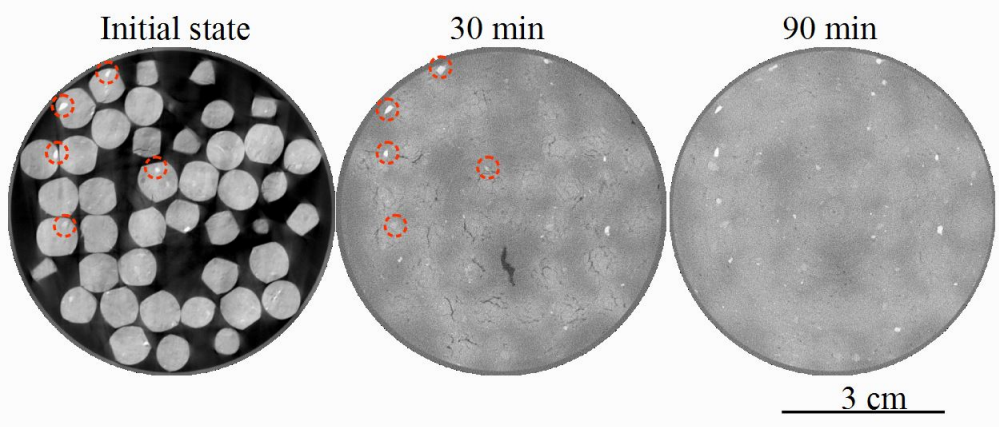


Fig. 9. Horizontal sections at 110 mm from the bottom of sample 1a. White points within the section correspond to the high density materials inserted into the mixture for image calibration.

440x189mm (72 x 72 DPI)

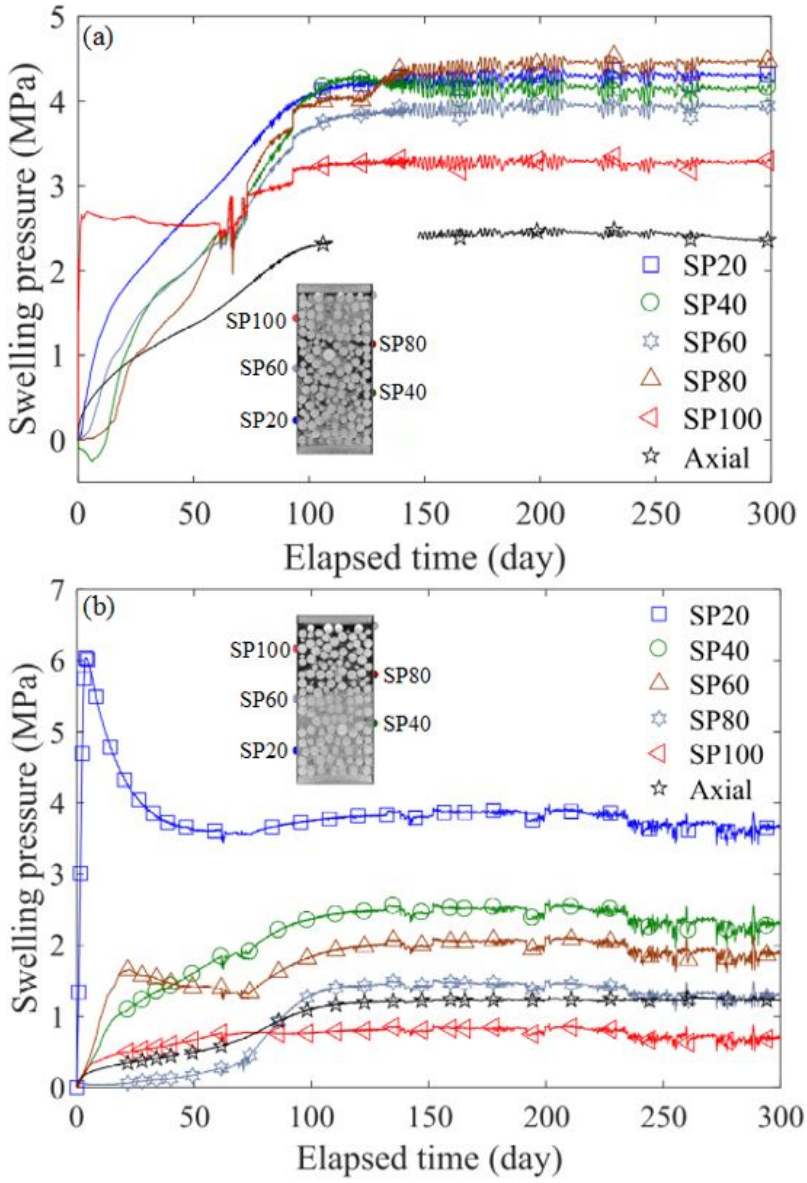


Fig. 10. Evolution of swelling pressure with time – results of mock-up tests - for (a) sample 1 with a proportion of 80-pellet/20-powder and (b) sample 2: proportion of 65-pellet/35-powder for the lower half and 100-pellet/0-powder for the upper half.

196x291mm (72 x 72 DPI)

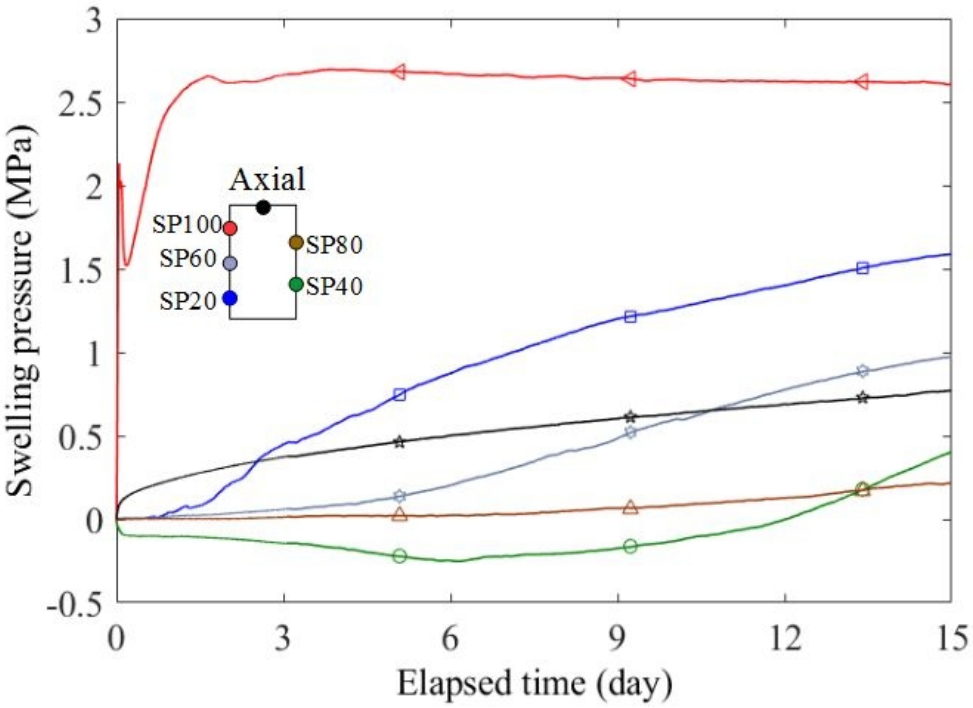


Fig11. Evolution of the swelling pressure in sample 1 – zoom on the first 15 days.

143x101mm (120 x 120 DPI)

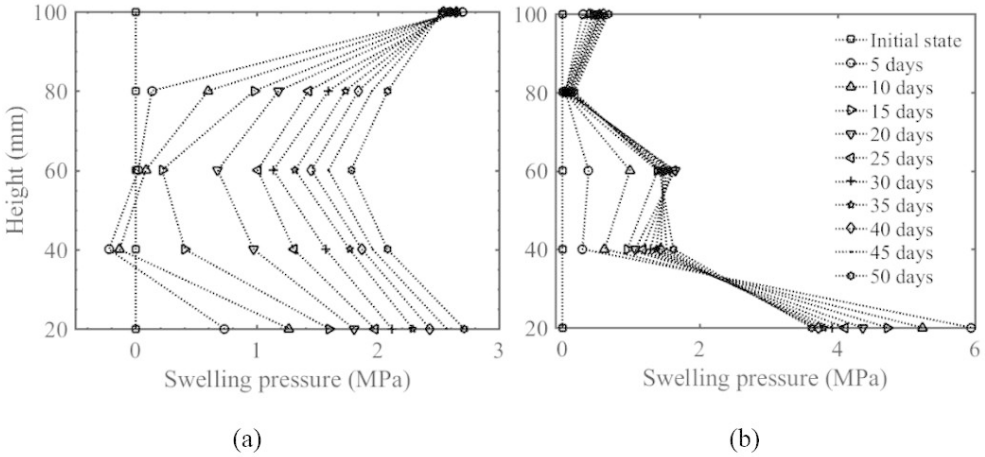


Fig. 12. Radial swelling pressure profiles in (a) sample 1 and (b) sample 2.

372x179mm (72 x 72 DPI)

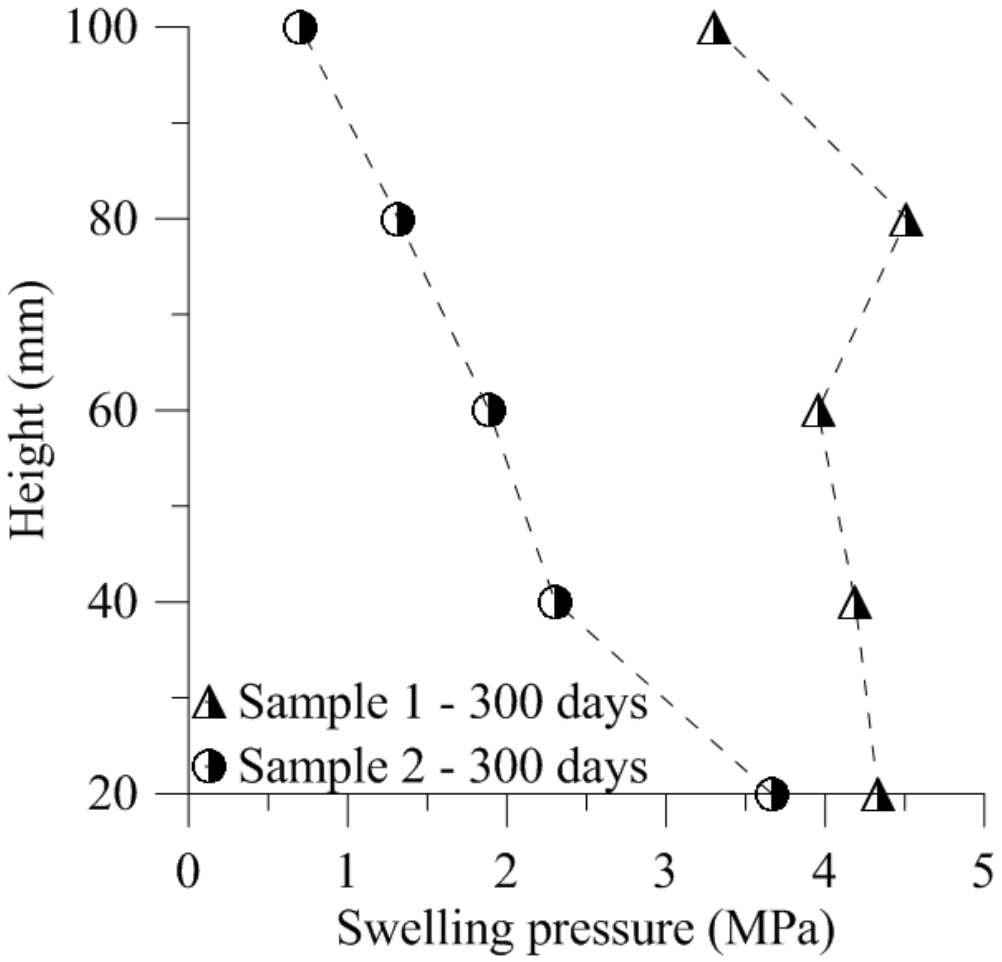


Fig. 13. Radial swelling pressure profiles after 300 days of hydration in samples 1 and 2.

153x147mm (100 x 100 DPI)

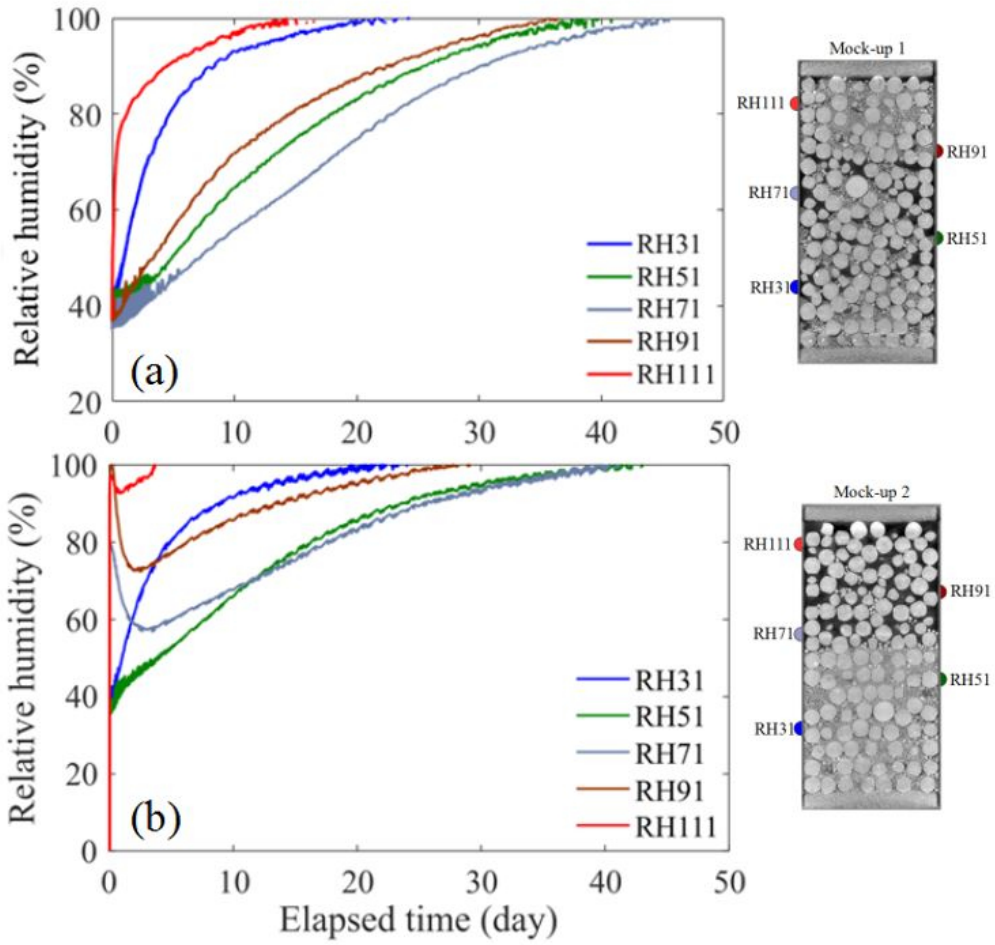


Fig. 14. Evolution of relative humidity in (a) sample 1 and (b) sample 2.

259x253mm (72 x 72 DPI)

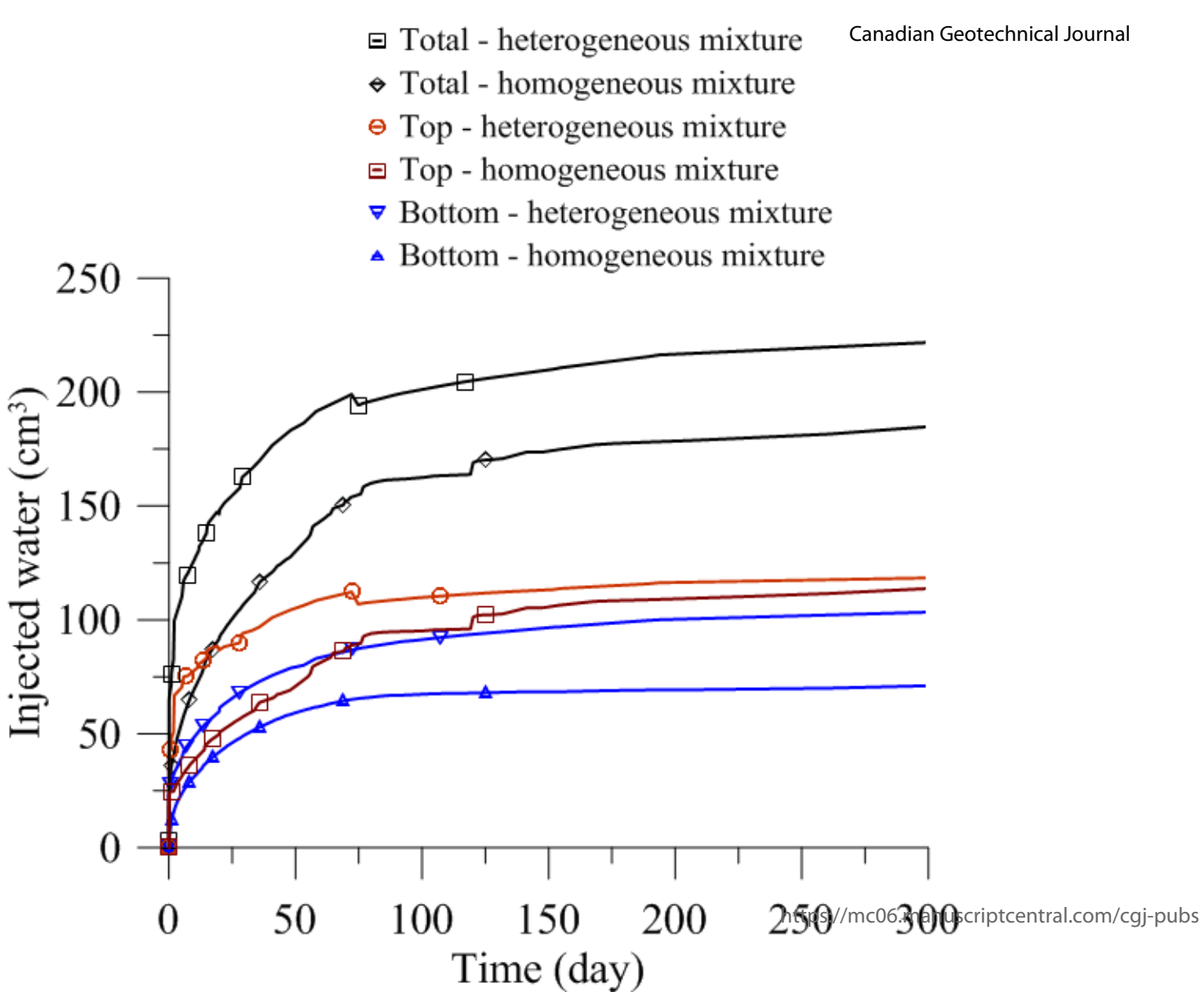


Fig. 11. Volumes of injected water into sample 1 and sample 2 while hydration.

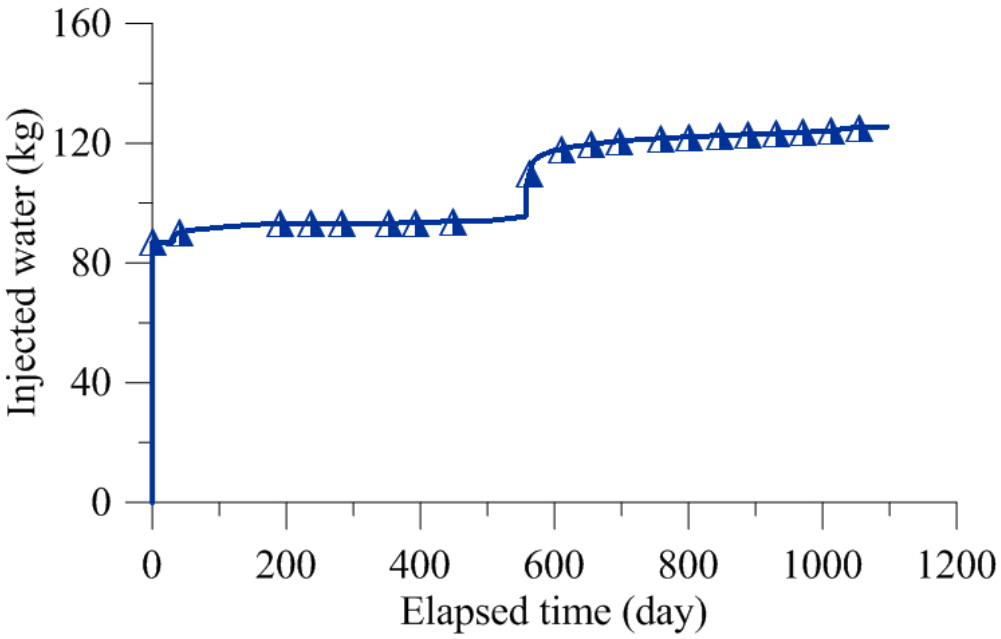


Fig. 16. Injected volume of water in the SEALEX in situ test PTN4.

189x120mm (100 x 100 DPI)

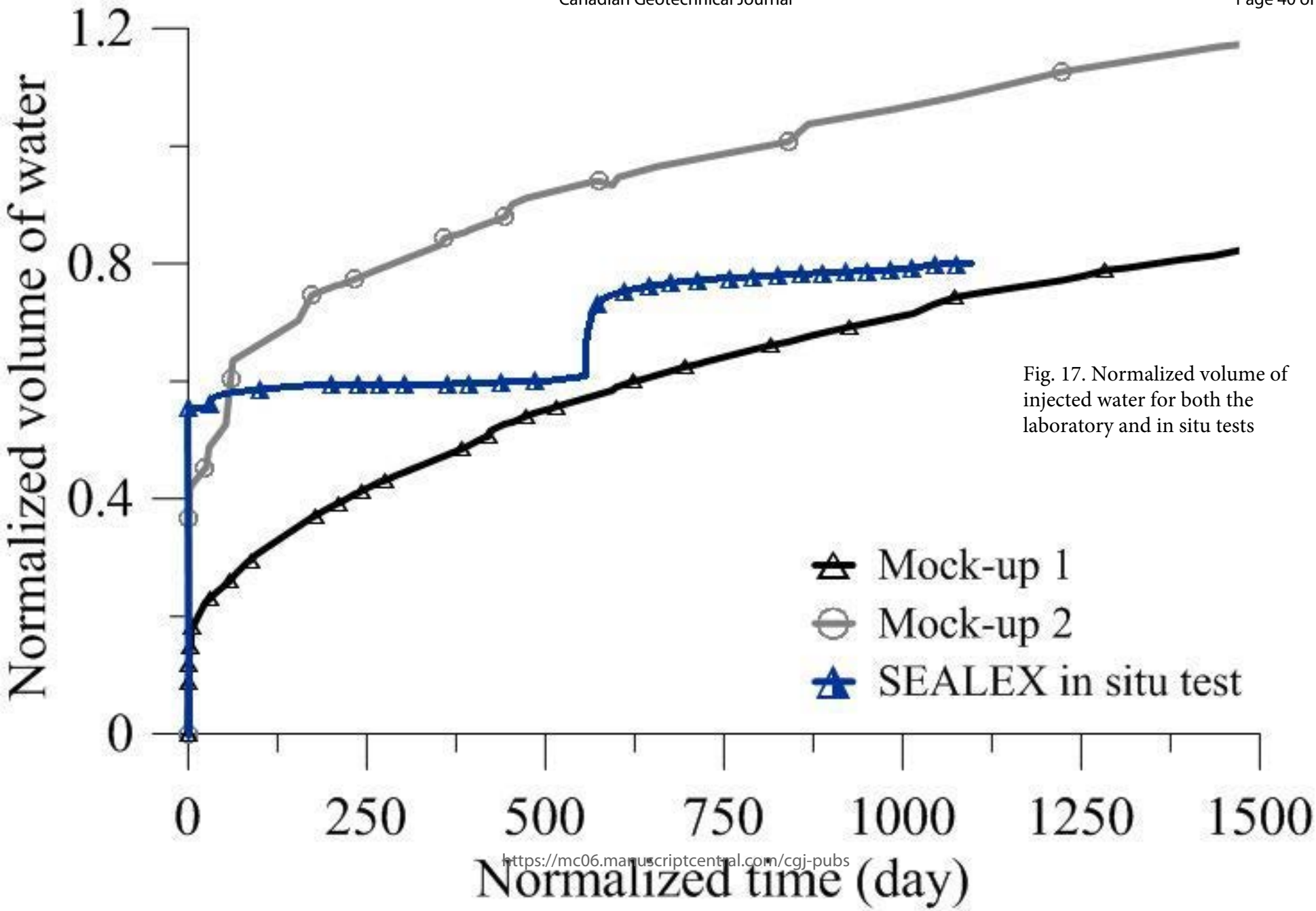


Fig. 17. Normalized volume of injected water for both the laboratory and in situ tests

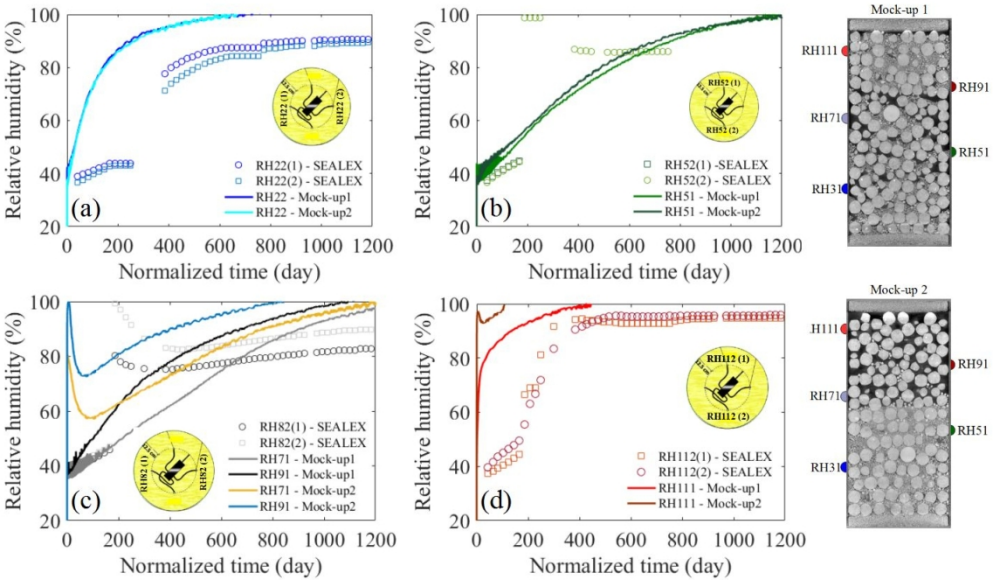


Fig. 18. Comparison of relative humidity results between SEALEX in-situ results and mock-up tests. (a) RH22; (b)RH52 for SEALEX test and RH51 for mock-up tests; (c) RH82 for mock-up tests, RH71 and RH91 for mock-up tests; (d) RH112 for SEALEX test, RH111 for mock-up tests.

503x295mm (72 x 72 DPI)

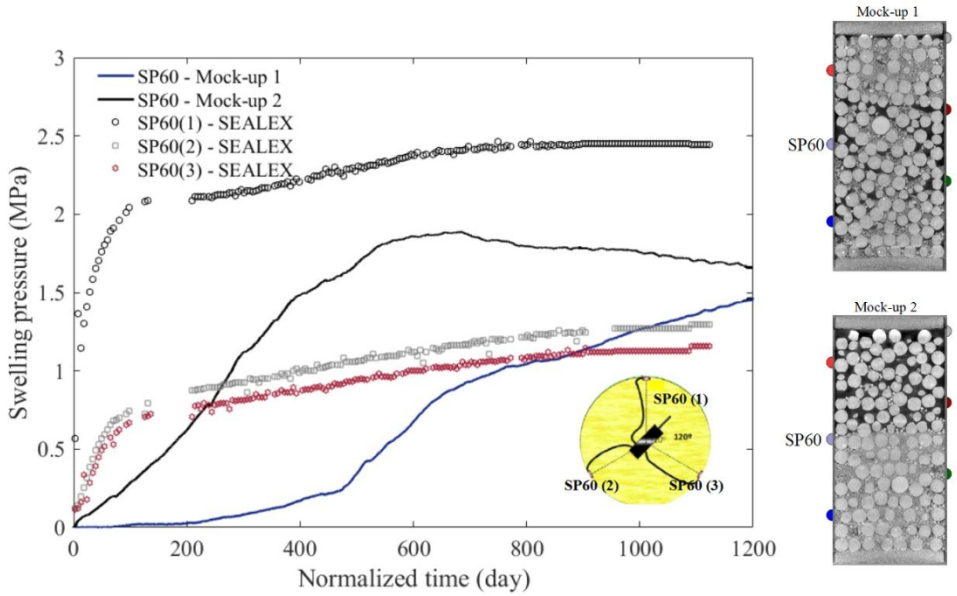


Fig. 19. Comparison of swelling pressure results at 60 mm from the bottom hydration front for SEALEX in-situ test and mock-up 1 test.

455x271mm (72 x 72 DPI)

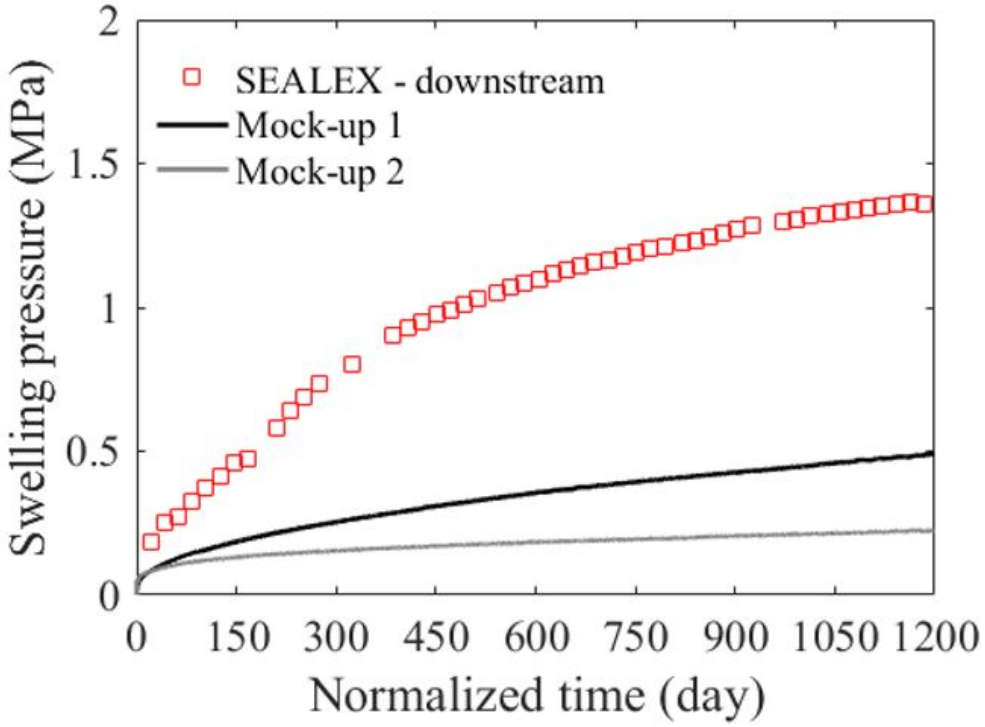


Fig. 20. Comparison of axial swelling pressure between SEALEX in-situ test and mock-up 1 test.

232x179mm (72 x 72 DPI)

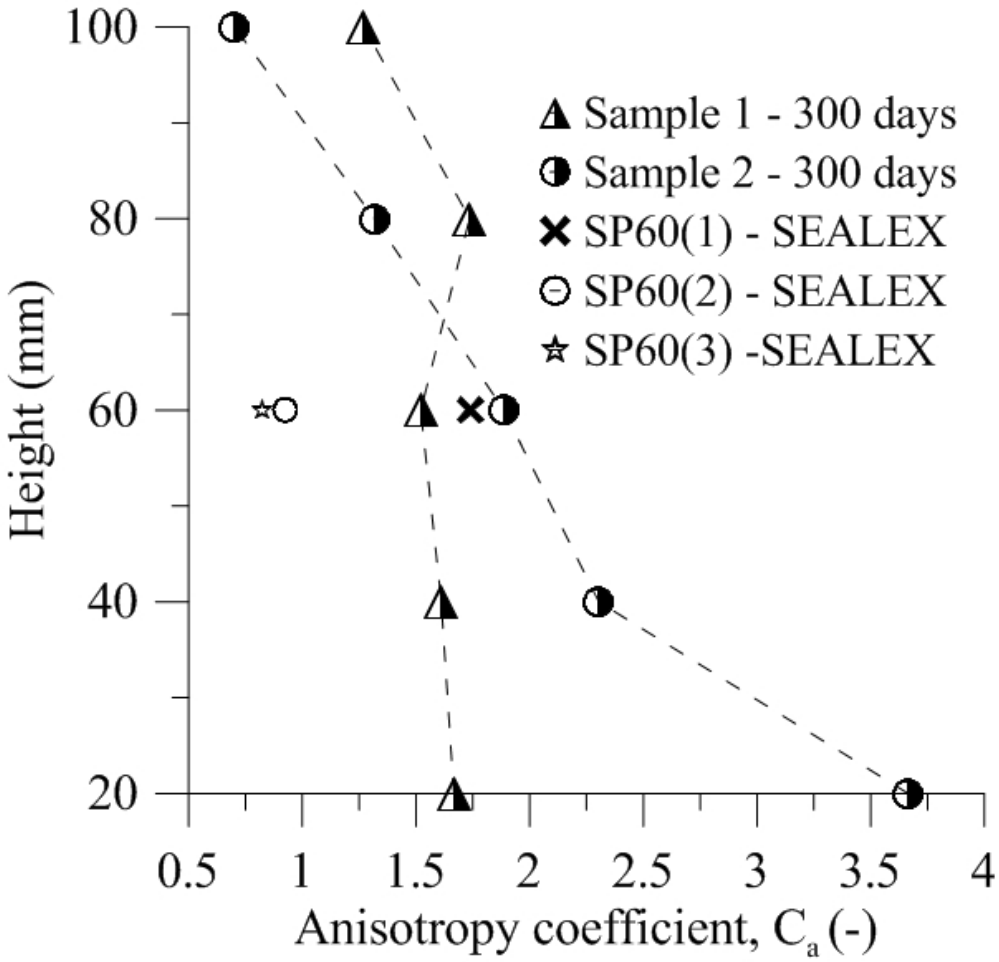


Fig. 21. Anisotropy coefficient Ca for mock-up tests and in situ SEALEX test.

153x148mm (100 x 100 DPI)

Table 1. Chemical composition of the synthetic water

| Components | $NaHCO_3$ | $Na_2SO_4$ | NaCl | KCl | $CaCl_2$ $2H_2O$ | $MgCl_2O6H_2O$ | $SrCl_26H_2O$ |
|---|---|---|---|---|---|---|---|
| Mass (g) per litre of solution | 0.28 | 2.216 | 0.615 | 0.075 | 1.082 | 1.356 | 0.053 |